
Figures and figure supplements

Probabilistic, spinally-gated control of bladder pressure and autonomous micturition by Barrington's nucleus CRH neurons

Hiroki Ito et al

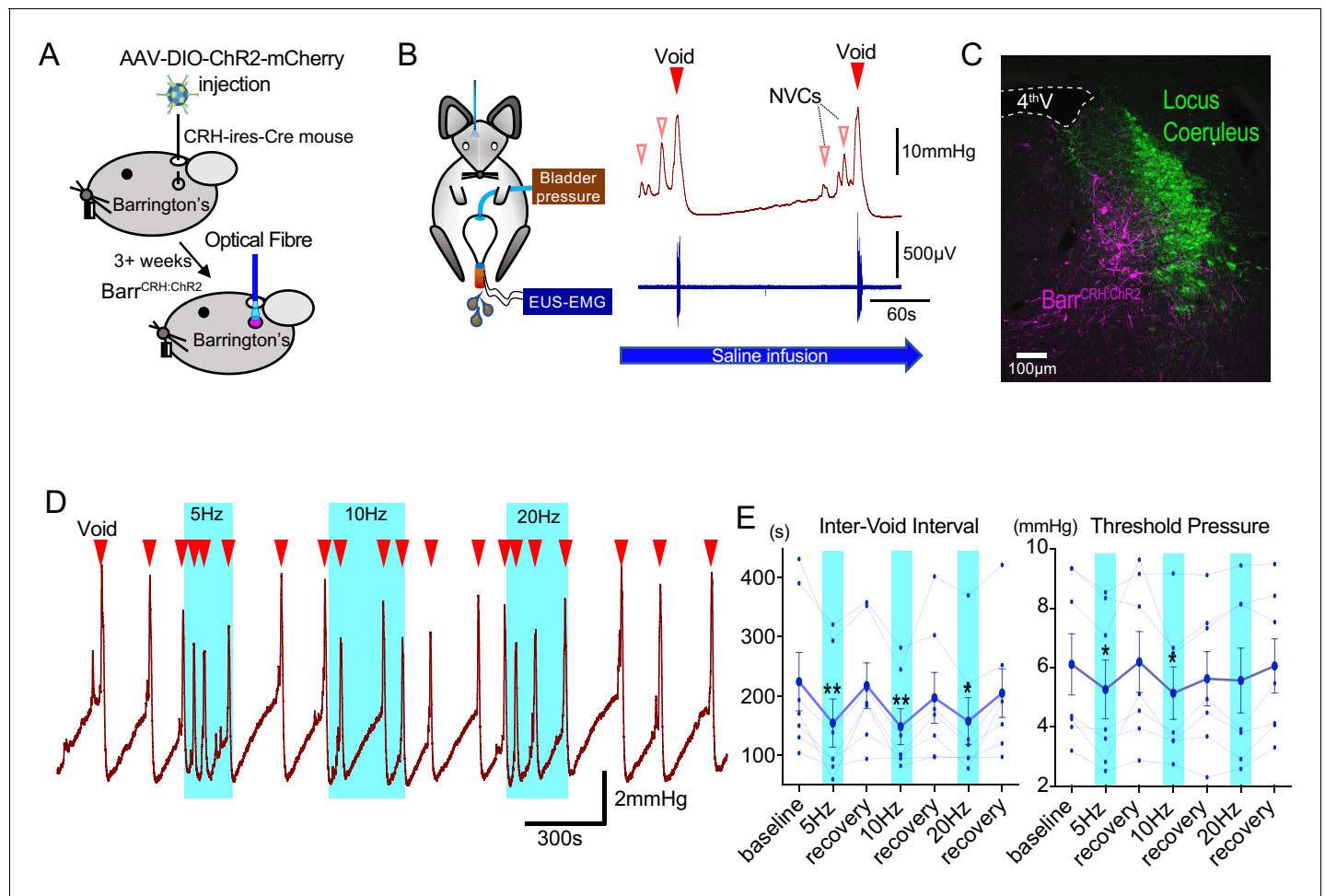


Figure 1. Optoactivation of Barr^{CRH} neurons shortens the micturition cycle. (A) AAV-DIO-ChR2-mCherry injection to dorsal pons in CRH^{Cre} mice followed after 3 weeks by opto-activation by light (465 nm) from an optical fibre. (B) In vivo recording in urethane anaesthetized mice with optical fibre positioned above Barrington's nucleus in the pons with bladder pressure and external urethral sphincter activity monitoring during the micturition cycle (with continuous bladder filling). (C) Post-hoc histology after stereotaxic injection of AAV-DIO-ChR2-mCherry demonstrating transduction of Barr^{CRH} neurons in sections of dorsal pons. Immunohistochemistry for mCherry (Magenta) shows transduced Barr neurons and Tyrosine hydroxylase (Green) marks the adjacent Locus Coeruleus. (D) Periods of maintained unilateral opto-activation of Barr^{CRH:ChR2} increased the frequency of micturition (light pulsed at 5, 10 and 20 Hz x 20 ms for three micturition cycles). (E) Continuous opto-activation (5, 10 and 20 Hz) reversibly shortened the inter-void interval ($n = 7$ mice). Similarly, the threshold for voiding was reversibly reduced with 5 and 10 Hz stimulation (Friedman test with Dunn's multiple comparisons to prior unstimulated state $*p < 0.05$, $**p < 0.01$, **Figure 1—source data 1**). NVC – Non-voiding contraction. Cystometrogram measures shown on **Figure 1—figure supplement 2**.

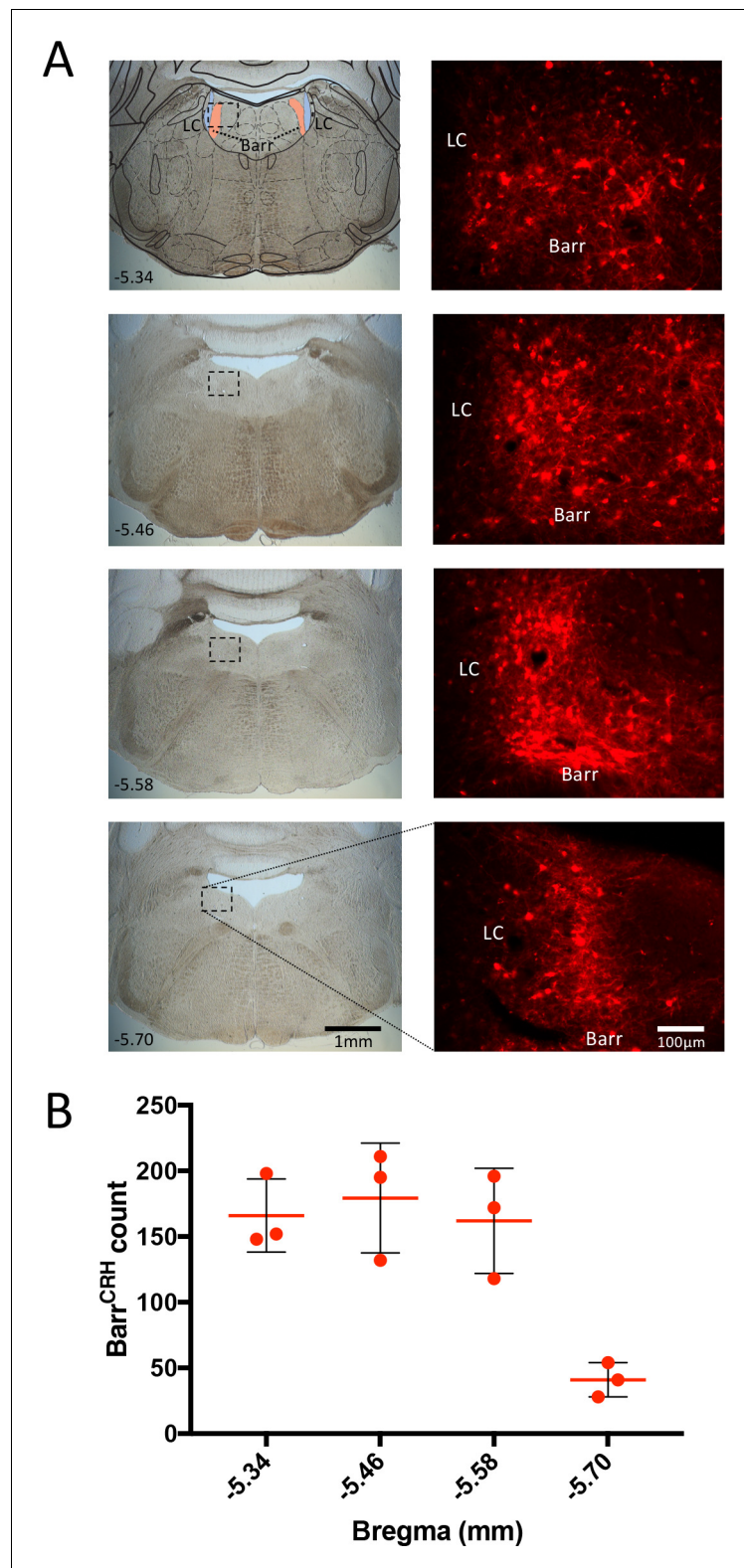


Figure 1—figure supplement 1. Histological verification of vector expression in Barrington's nucleus. (A) Following injection of AAV-EF1 α -DIO-ChR2-mCherry to CRH^{Cre} mice, expression of mCherry was seen in the dorsal pons (Bregma -5.34 to -5.7) in Barrington's nucleus (overlaid atlas section from *Paxinos and Franklin, 2008*). (B) Cell counts of transduced neurons in Barrington's nucleus from three mice showing mean \pm SD. Immuno- for mCherry with Alexa594 conjugated secondary antibody. LC – locus coeruleus, Barr – Barrington's nucleus.

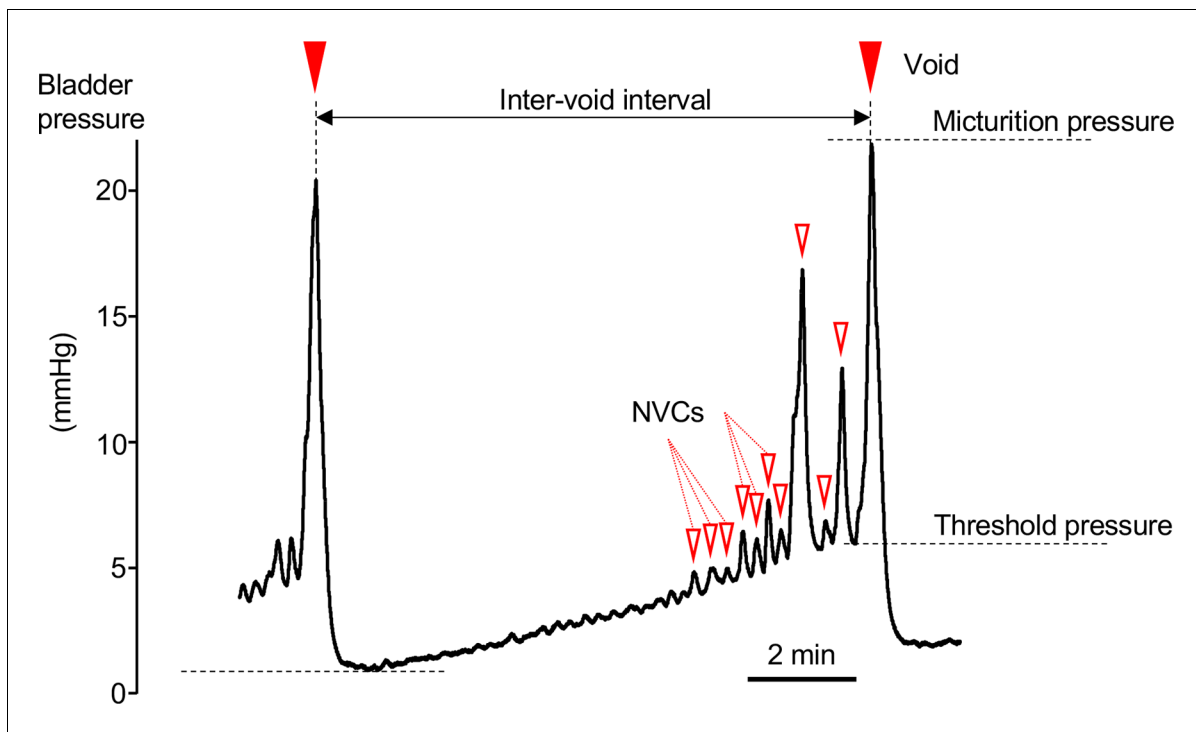


Figure 1—figure supplement 2. Cystometrogram. Typical cystometrogram trace showing two complete voids and the intervening storage phase in response to a continuous infusion of saline to the bladder. The measured variables are indicated on the bladder pressure trace:

- Inter-void interval as time between successive voids.
- Basal pressure was taken as the lowest bladder pressure reached after a void.
- Voiding threshold was the bladder pressure at the point of initiation of voiding.
- Micturition pressure was the peak bladder pressure achieved during a void.
- Non-voiding contractions (NVCs, open triangles marking some of the events) were identified as discrete increases in bladder pressure (>0.1 mmHg) observed during the filling phase.

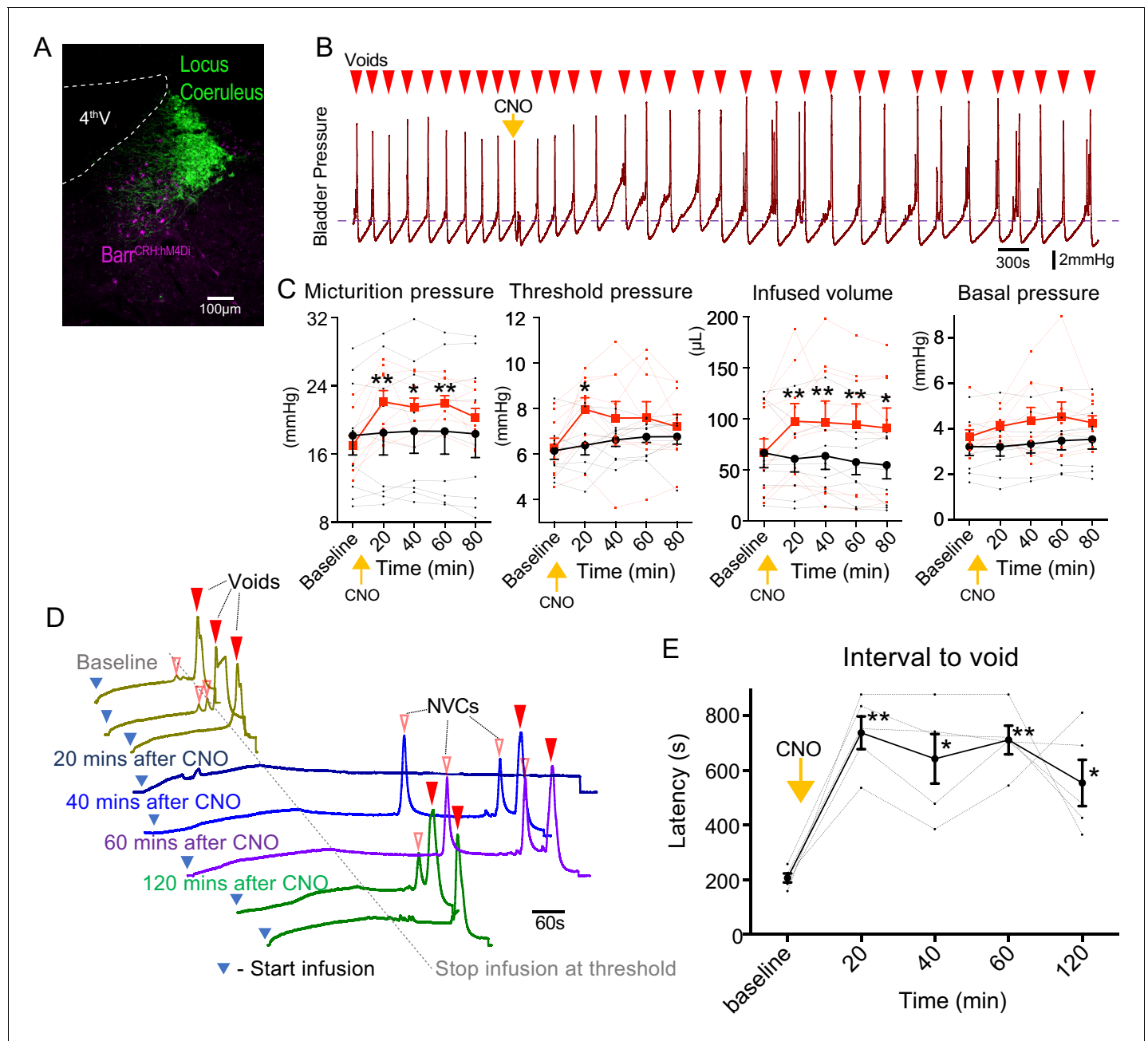


Figure 2. Chemogenetic inhibition of Barr^{CRH} neurons prolongs the micturition cycle. (A) Transduction of Barr^{CRH} with inhibitory DREADD using AAV-DIO-hM4Di-mCherry demonstrated with immunocytochemistry for mCherry (magenta) and Tyrosine hydroxylase (green) to mark the Locus Coeruleus. (B) Administration of the DREADD ligand CNO (5 mg/kg, i.p.) slowed the frequency of micturition seen with continuous saline infusion to the bladder. (C) The chemogenetic inhibition of Barr^{CRH:hM4Di} neurons caused an increase in the voiding threshold ($129.7 \pm 8.9\%$), volume infused before void ($161.9 \pm 16.9\%$) and micturition pressure ($131.7 \pm 6.9\%$) compared to baseline (RM-ANOVA with Holm-Sidak's post hoc, * $p < 0.05$, ** $p < 0.01$) unlike control mice (Barr^{CRH:ChR2}, $n = 9$ per group) where CNO was without significant effect. In each case this CNO effect peaked around 20 min after administration and reversed slowly. (D) Using an intermittent bladder infusion protocol (to a maximum bladder pressure of 15 mmHg) CNO administration inhibited voiding with (E) a large increase in the latency to void (time after start of infusion) – equivalent to urinary retention ($n = 5$) (RM-ANOVA with Holm-Sidak's post hoc, * $p < 0.05$, ** $p < 0.01$). Source data in **Figure 2—source data 1**.

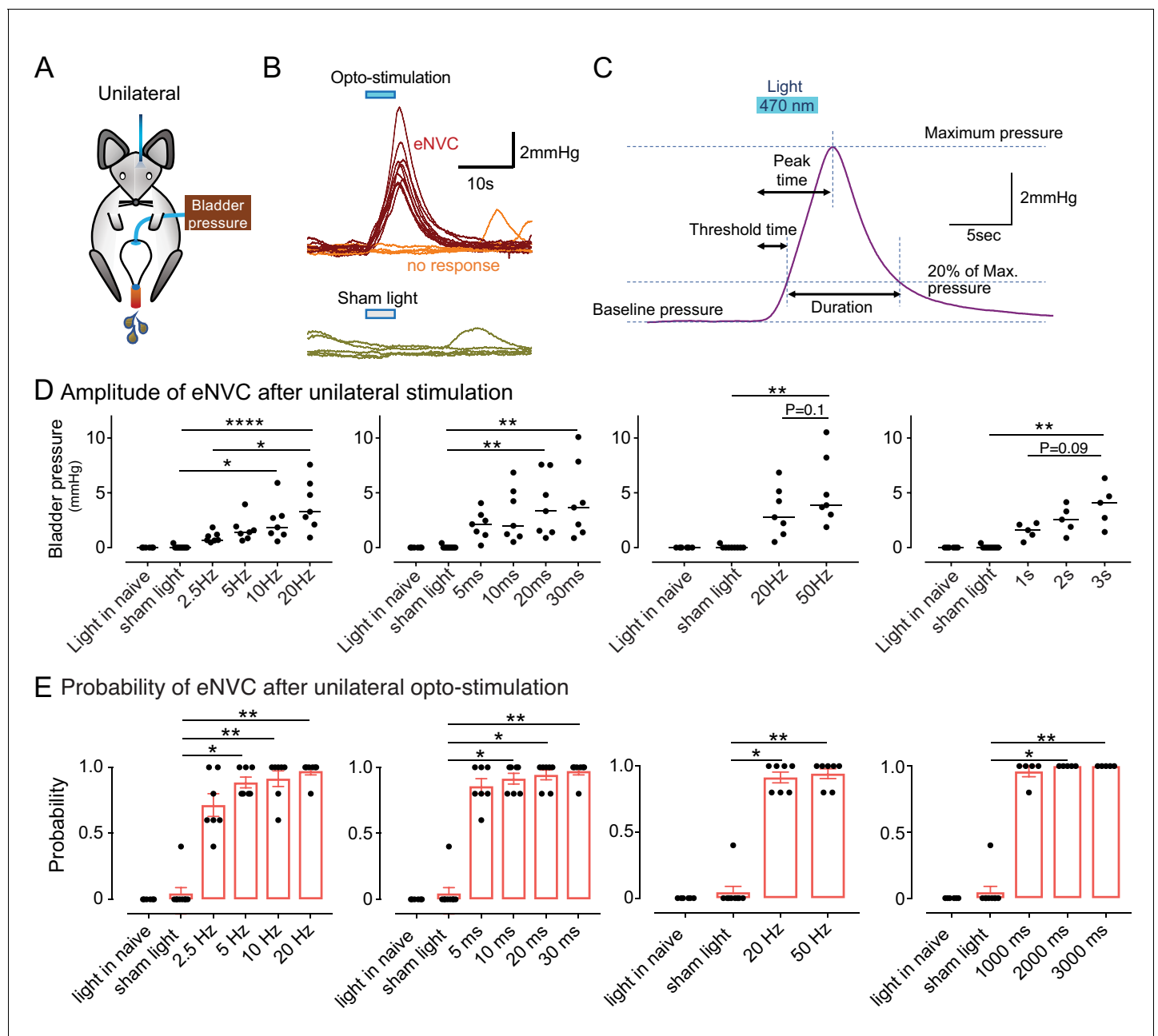


Figure 3. Phasic optoactivation of Barr^{CRH} evokes bladder contractions. (A) Bladder pressure recordings with unilateral opto-activation (B) Phasic opto-activation (20 ms x 20 Hz, 5 s) of Barr^{CRH} neurons evoked non-voiding contractions (eNVCs, with the bladder ~half full, static). These eNVCs had a stereotyped shape and a relatively constant latency. In addition, there were 'failures' where no response was evoked by an identical stimulus. (C) Parameters of Barr^{CRH} evoked non-voiding contractions. Threshold calculated at 20% of the amplitude, duration was measured at the threshold pressure. The latency was taken as the time from start of stimulation for the pressure to reach threshold. (D) The amplitude of eNVC increased with stimulation frequency (pulse length 20 ms for 5 s) and pulse duration (at 20 Hz for 5 s) (n = 7 mice). Higher frequencies of stimulation (50 Hz x 10 ms) did not substantially increase eNVC amplitude. Single longer light pulses (1–3 s) could also generate graded eNVCs. (E) The probability of generating an eNVC increased with stimulation frequency (pulse length 20 ms for 5 s) and pulse duration (frequency 20 Hz for 5 s). Longer light pulses (1–3 s) also reliably generated eNVCs. (RM-ANOVA with Dunnett's post hoc or Friedman's test, *p<0.05, **p<0.01, ****p<0.0001). Source data in **Figure 3—source data 1**.

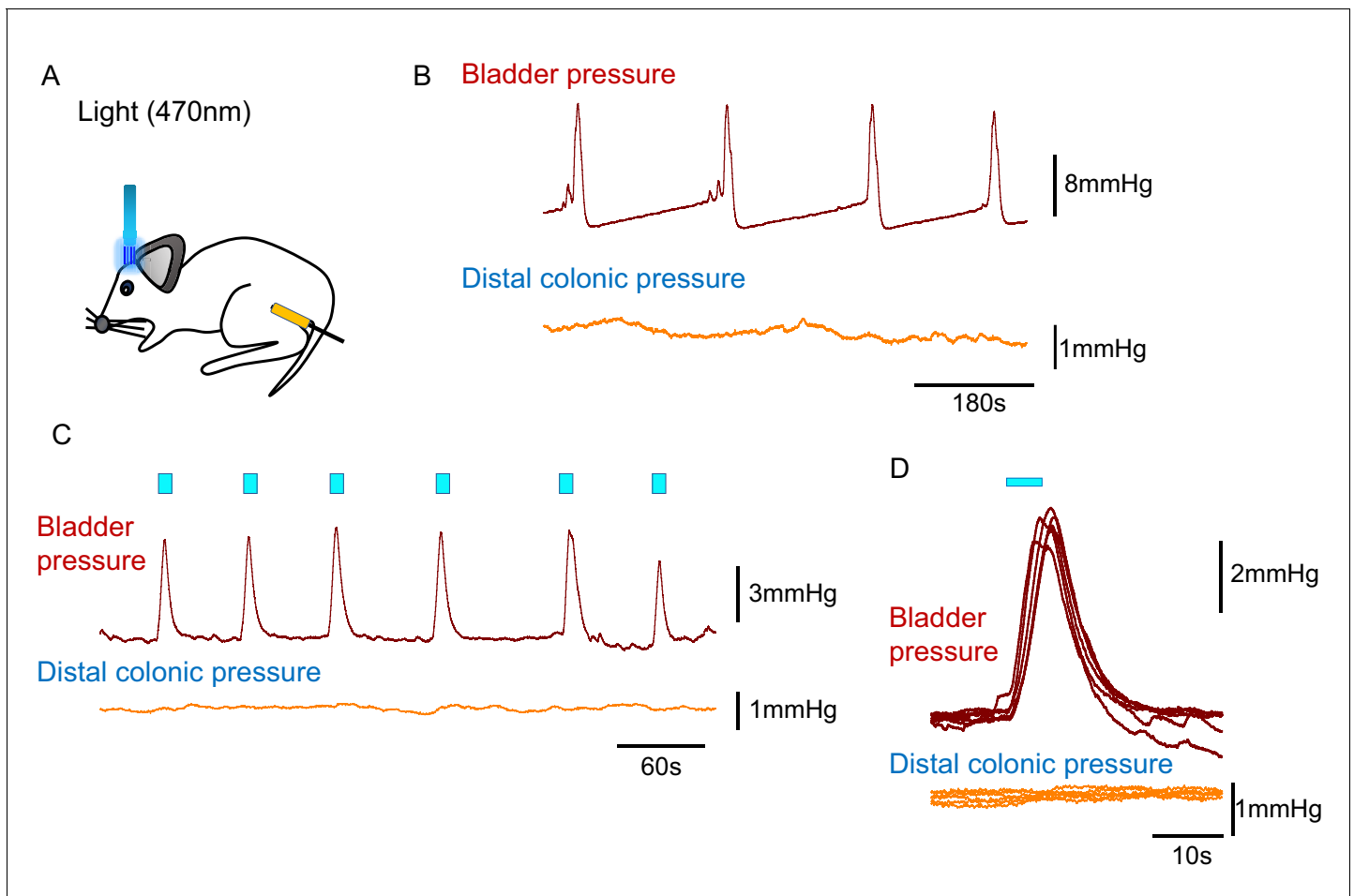


Figure 3—figure supplement 1. Barr^{CRH} optoactivation does not cause contraction of the distal colon. (A, B) Simultaneous recording of bladder pressure and rectal pressure with an intraluminal balloon showed no clear relationship between colonic pressure and the micturition cycle during continuous filling cystometry. (C, D) Similarly, although opto-activation (20 ms x 20 Hz for 5 s) of Barr^{CRH} generated bladder eNVCs, there was no corresponding response in the distal colon.

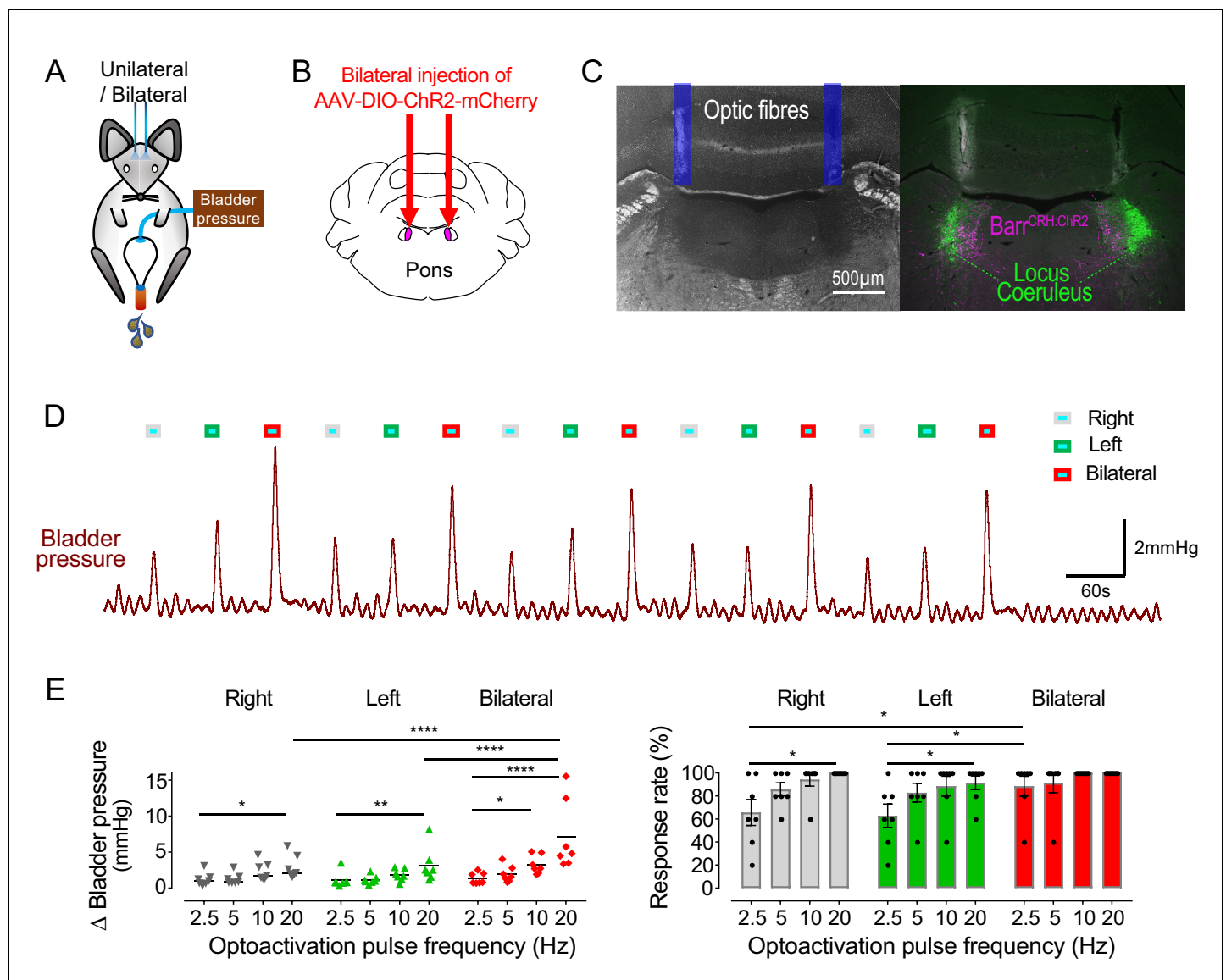


Figure 4. Bilateral phasic optoactivation of Barr^{CRH} evokes larger non-voiding contractions than unilateral optoactivation. (A) Bladder pressure recordings with unilateral or bilateral opto-activation following (B) bilateral injection of AAV-DIO-ChR2-mCherry. (C) Confirmation of bilateral Barr^{CRH}:ChR2 transduction and optic fibre targeting (immuno for mCherry – magenta and TH - green). (D) Bladder pressure response showing the effect of unilateral or bilateral phasic opto-activation (20 ms x 20 Hz, 5 s) of Barr^{CRH} neurons evoked non-voiding contractions (eNVCs, with the bladder ~half full, static). A comparison of the effects of unilateral versus bilateral stimulation (E) showed that bilateral stimulation evoked larger events and with an increased reliability than either side alone (each point represents data from a single mouse, *n* = 7 mice, RM-ANOVA with Dunnett's post hoc or Friedman's test, **p*<0.05, ***p*<0.01, *****p*<0.0001). Source data in **Figure 4—source data 1**.

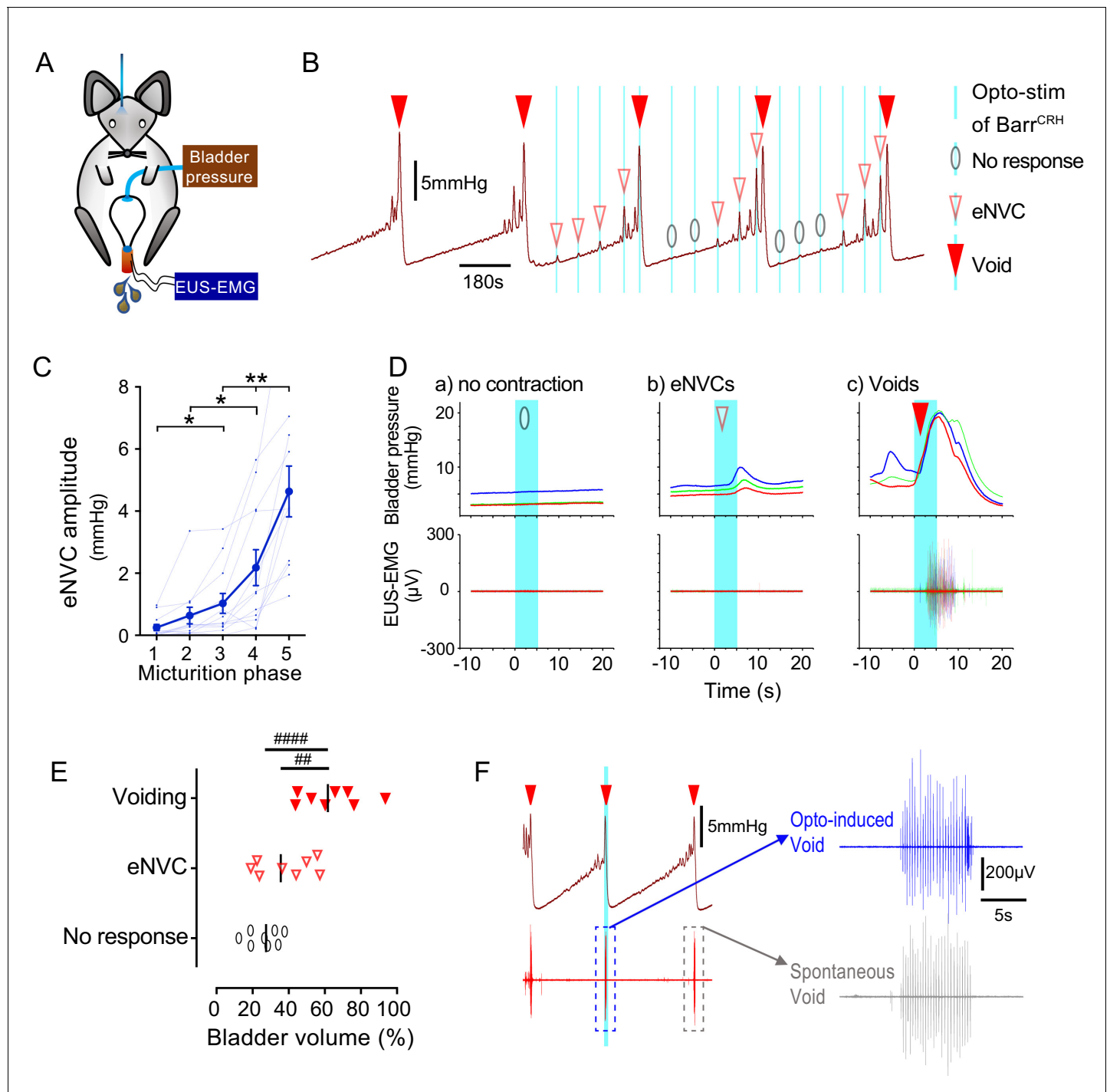


Figure 5. Dynamics of Barr^{CRH} evoked events through the micturition cycle. (A) Experimental set-up with unilateral opto-activation of Barr^{CRH} neurons. (B) Continuous infusion cystometry with episodic opto-activation (20 Hz x 20 ms for 5 s) applied at different phases of the micturition cycle generates eNVC of incrementing amplitude as the cycle progresses. (C) There is a substantial increase in the amplitude of the eNVC as the micturition cycle progresses (17.0 ± 3.9 fold comparing eNVC from the 2nd and 5th quintiles of the cycle) (RM one-way ANOVA followed by Dunnet's test, * $P < 0.05$, ** $P < 0.01$). (D) Overlaid bladder pressure responses to the same optogenetic stimulus applied (x3) at different phases of the cycle can trigger either no response or eNVCs or full voiding contractions that show a stereotyped morphology and latency. (E) Analysis of the stage of the voiding cycle where each type of response was triggered showed that voiding contractions were significantly more likely to be evoked later in the voiding cycle (each symbol represents the average position of such events in each mouse, $n = 8$) (RM one-way ANOVA with Tukey's test, ### $P < 0.01$, #### $P < 0.0001$). (F) The bursting pattern of EUS activity was similar with both Barr^{CRH}-evoked and spontaneous voids. Source data in **Figure 5—source data 1**.

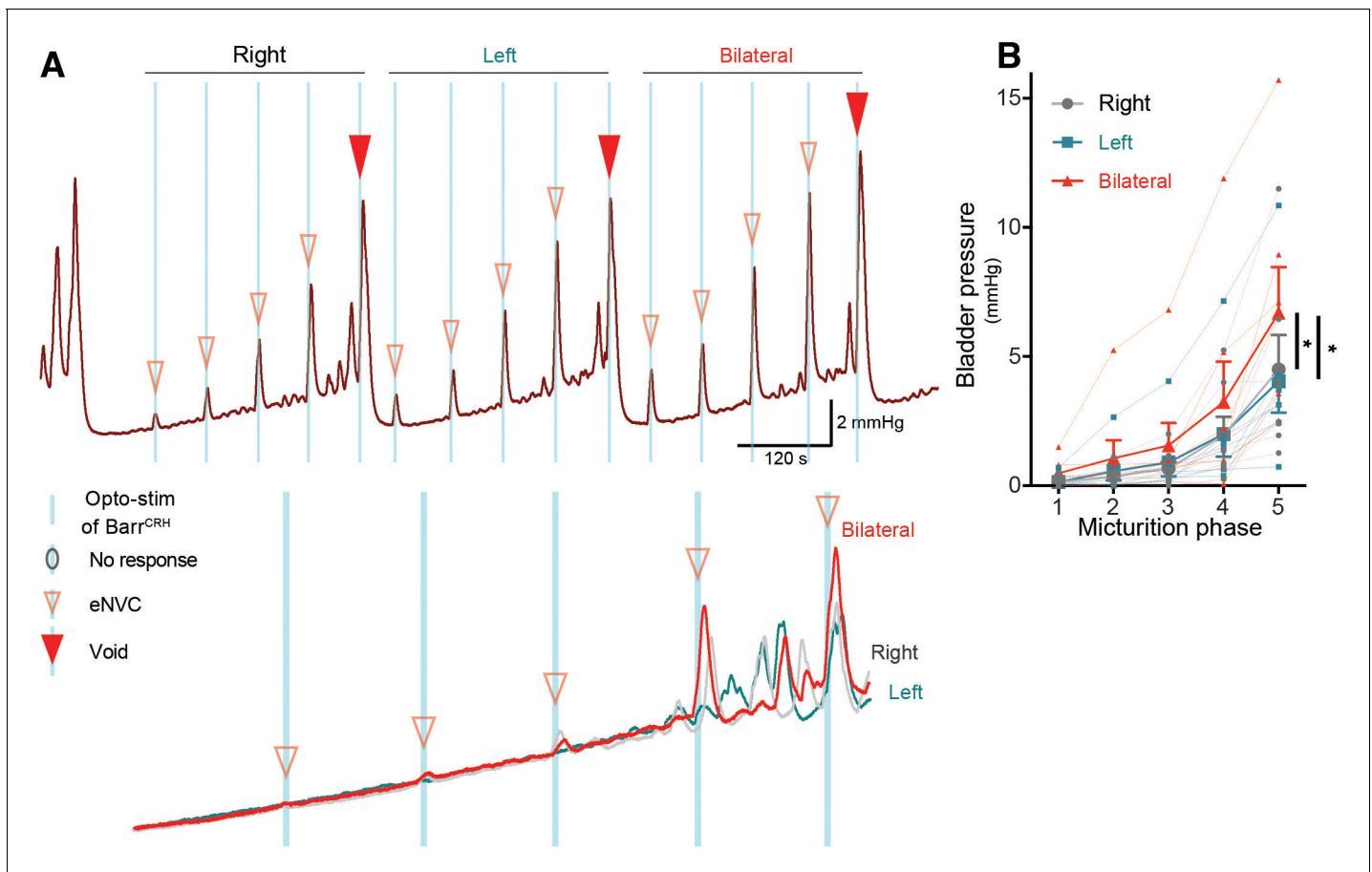


Figure 5—figure supplement 1. Dynamics of bilateral Barr^{CRH} evoked events through the micturition cycle. **(A)** Comparison of unilateral with bilateral opto-activation of Barr^{CRH} neurons during continuous filling cystometry showing the graded increase in eNVC amplitude with phase of the micturition cycle and the augmented response to bilateral stimulation. **(B)** Bilateral stimulation evoked larger eNVC, an effect that is more pronounced later in the micturition cycle ($n = 7$ mice). (* - $p < 0.05$, Related samples Friedman's two way-ANOVA by ranks.). Source data in **Figure 5—figure supplement 1—source data 1**.

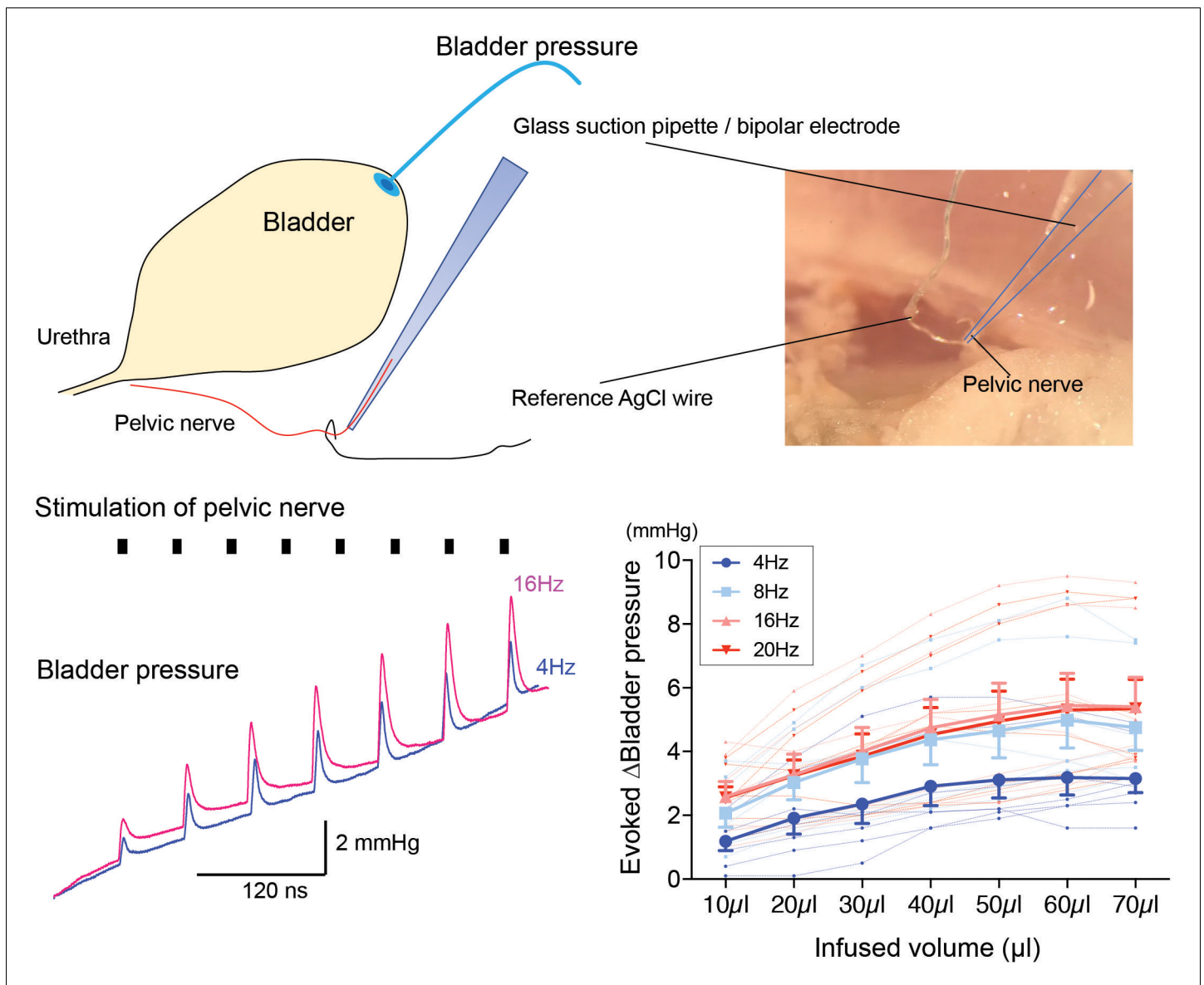


Figure 5—figure supplement 2. Dependence of pressure response to electrical stimulation of the pelvic nerve on bladder filling. Using the pithed decerebrate arterially perfused mouse preparation ($n = 7$), the bladder pressure was monitored while the pelvic nerve was stimulated using a bipolar suction electrode (10V, 4–20 Hz, train 3 s). Pelvic nerve stimulation evoked pressure responses that were dependent on stimulation frequency and on the degree of bladder distension. Source data in **Figure 5—figure supplement 2—source data 1**.

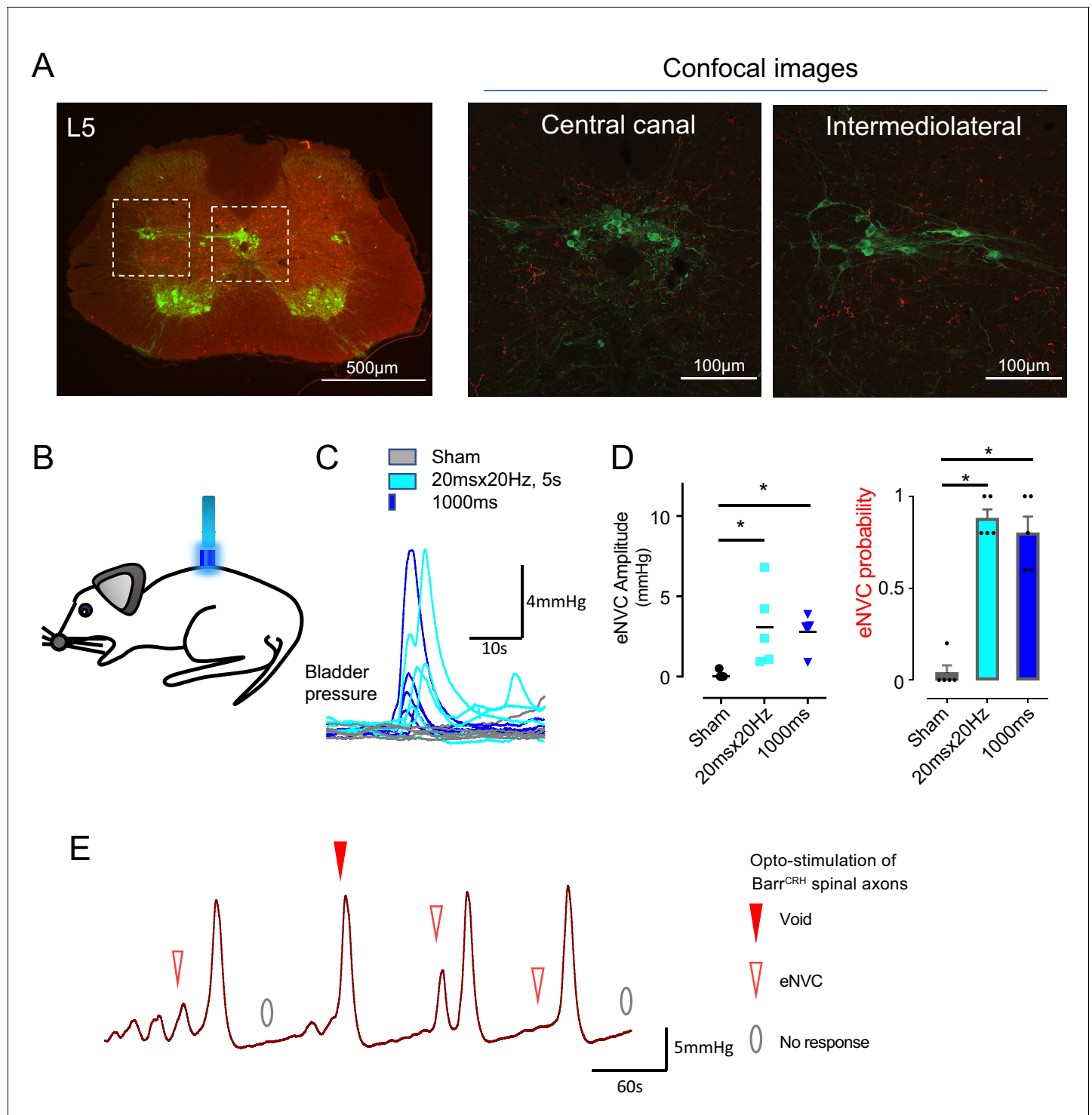


Figure 6. Spinal opto-activation of Barr^{CRH} axons generates eNVC and voids. (A) Unilateral transduction of Barr^{CRH} neurons with AAV-EF1 α -DIO-ChR2-mCherry. Spinal L5 section had immunocytochemistry for mCherry (red) and Choline acetyltransferase (green) to label filled Barr^{CRH} axons and somatic and autonomic motoneurons. The Barr^{CRH} axons show a lateralised distribution targeting the territory of parasympathetic preganglionic neurons at L5 (B) The spinal cord was exposed at the vertebral level of T11-12 and illuminated from an optic fibre placed above the cord. (C) Opto-activation (20 Hz x 20 ms for 5 s or single 1 s pulse) generated eNVCs (Related samples Friedman's test by ranks). (D) There was no difference in the eNVC in terms of amplitude or reliability between the two opto-stimulus patterns (n = 5 mice). (E) Opto-stimulation (20 Hz x 20 ms for 5 s) during continuous filling cystometry generated full voiding contractions as well as eNVCs. Source data in **Figure 6—source data 1**.

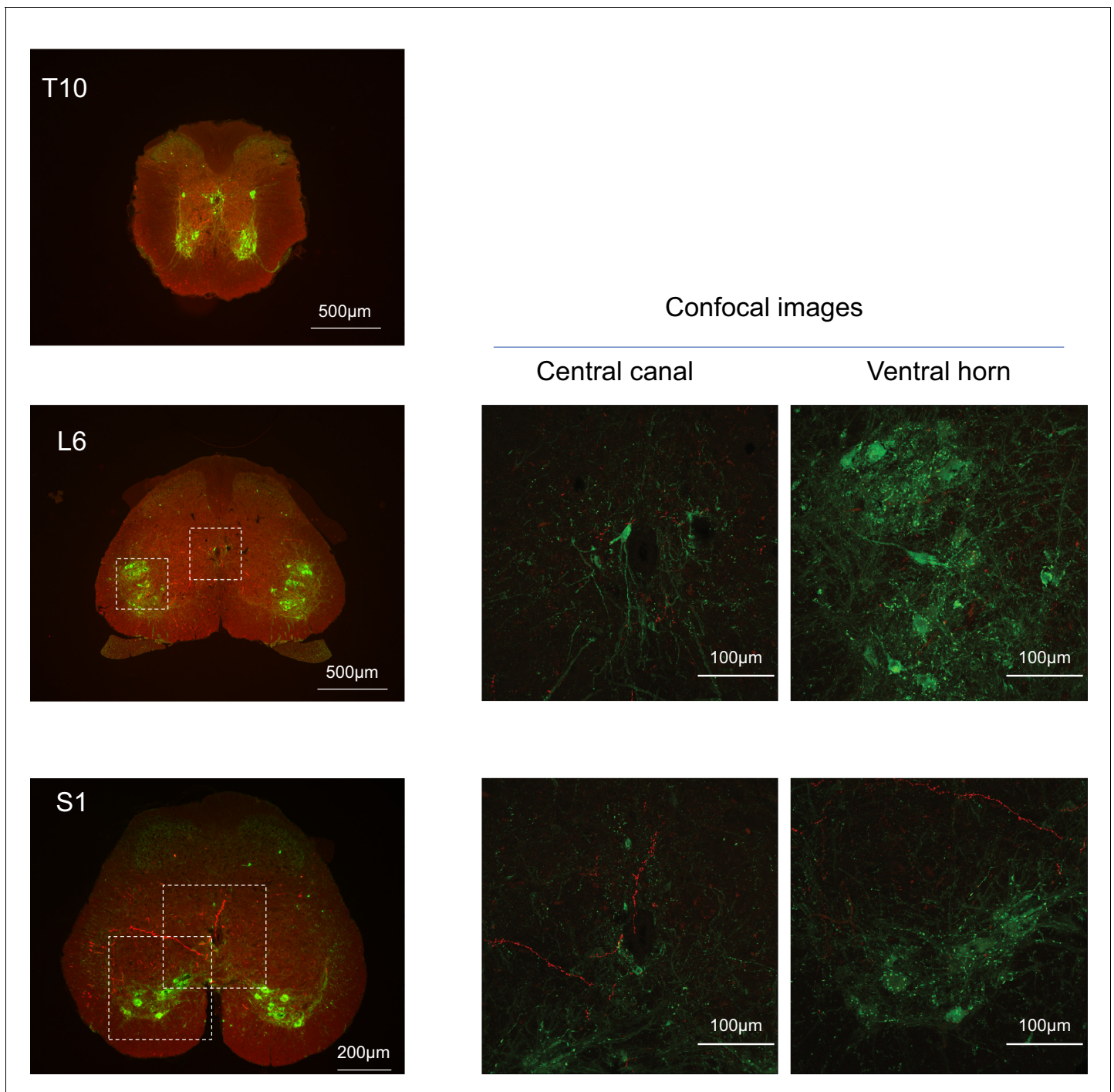


Figure 6—figure supplement 1. Spinal projections of Barr^{CRH} axons. Following unilateral transduction of Barr^{CRH} neurons with AAV-EF1α-DIO-ChR2-mCherry, transverse spinal cord sections (30 μm) were cut from T10-S1 segments. Sections were processed for fluorescence immunocytochemistry for mCherry (red) and Choline acetyltransferase (green) to label filled Barr^{CRH} axons and somatic and autonomic motoneurons, respectively. These are represented as widefield and confocal images of blow-outs. The Barr^{CRH} axons show a lateralised distribution and can be seen to target the territory of parasympathetic preganglionic neurons at L6 as well as in the ventral horn area in S1. Note the absence of labelling close to somatic motoneurons and the sympathetic preganglionics at T10.

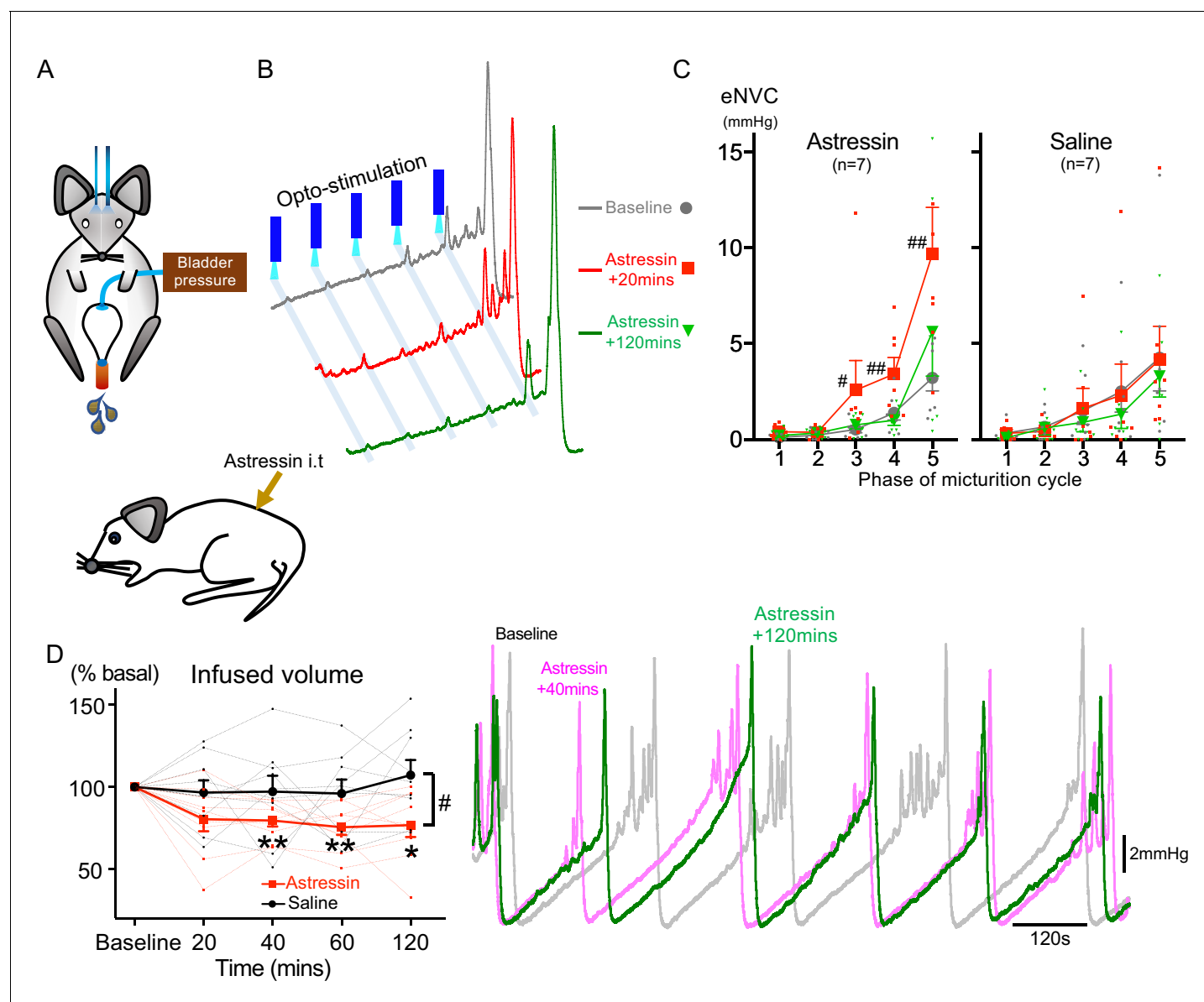


Figure 7. Spinal CRH inhibits the bladder response to Barr^{CRH} neuronal optoactivation. (A) Assessment of the influence of intrathecal Astressin (CRH antagonist) on the bladder pressure response to bilateral optoactivation of Barr^{CRH} neurons. (B) Intrathecal Astressin (5 μ g) reversibly increased the amplitude of Barr^{CRH} eNVC ($n = 7$ mice). (C) Summary data for the action of intrathecal Astressin on eNVC (versus vehicle control) showing that the augmentation of amplitude was particularly marked towards the end of the micturition cycle (Related samples Friedman's test by ranks, #-P < 0.05, ##-P < 0.01). (D) Even without Barr^{CRH} opto-stimulation Astressin reversibly increased the frequency of voiding compared both to baseline and an intrathecal vehicle control group ($n = 9$) (vs baseline with related samples Friedman's test by ranks and vs vehicle with Mann-Whitney U test, *-P < 0.05, **-P < 0.01). Source data in **Figure 7—source data 1**.

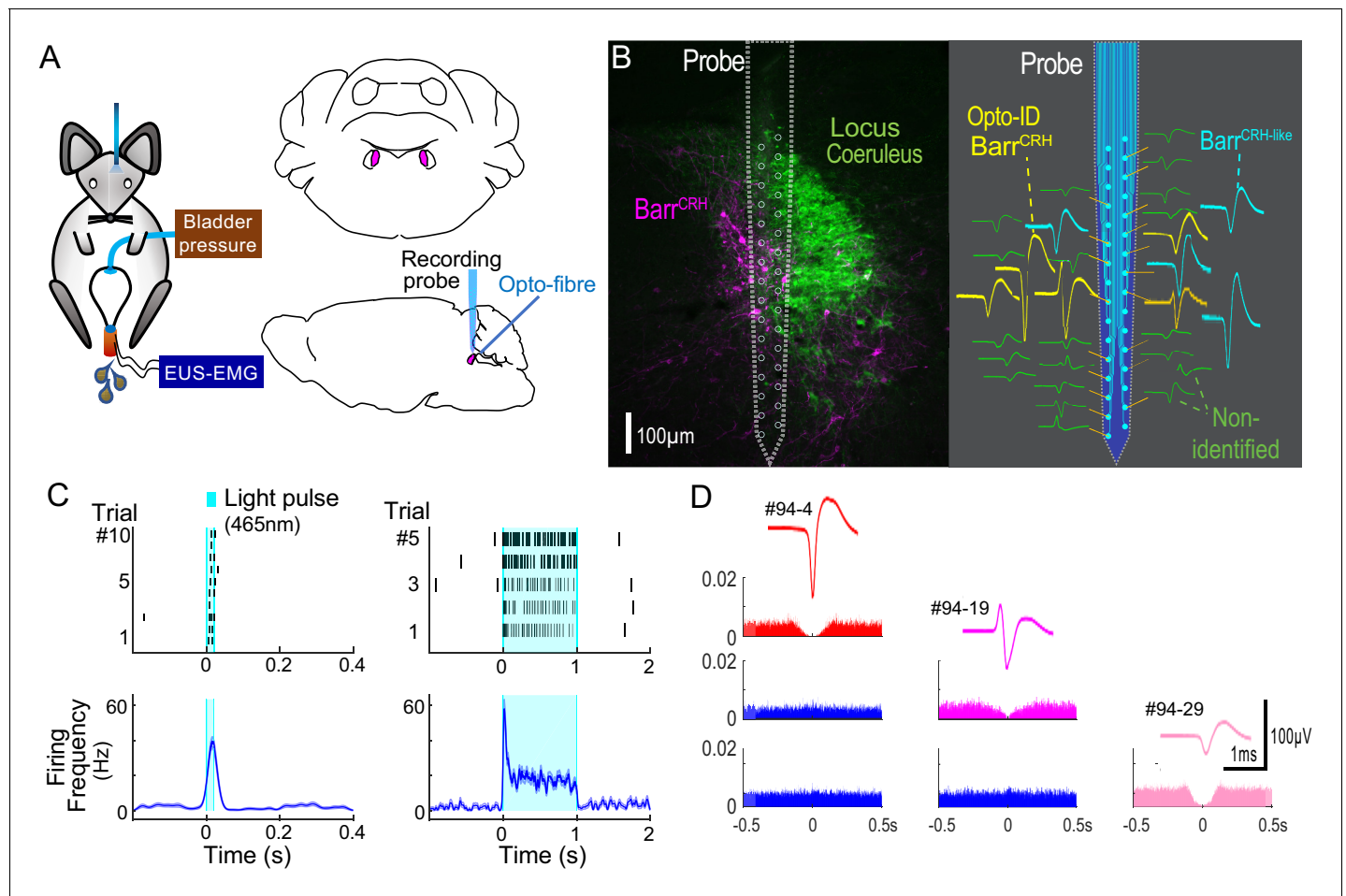


Figure 8. Multiunit recordings of identified Barr^{CRH} neurons. **(A)** Schematic with unilateral stimulation and recording of Barrington's nucleus with simultaneous bladder and EUS monitoring. **(B)** Immunohistochemistry (mCherry - magenta and TH - green) confirming the position of the recording electrode (shown to scale and with its tip at the end of the histological track). The spike waveforms of individual units are shown schematically adjacent to their probe recording site. Note that the Barr^{CRH} neurons (yellow) are clustered in sites located within Barrington's nucleus whereas the non-identified neurons (green) lie above and below the level of Barrington's nucleus. A third population of non-optoidentified neurons is shown in blue (labelled Barr^{CRH-like}) whose firing pattern closely resembled the Barr^{CRH} neurons **(C)** Barr^{CRH} neurons were optoidentified by a short latency response to a brief light pulse (20 ms) data shown for a single representative unit top left. The population response of identified Barr^{CRH} neurons shown below ($n = 12$, smoothed average firing rate curve generated by convolution of spikes with a Gaussian of SD 10 ms). The response to a 1 s light pulse is shown to the right with the same single unit and the population response from all Barr^{CRH} neurons. Note that they showed an initial high frequency response that decayed to a plateau of ~20 Hz likely reflecting the kinetics of ChR2 currents. **(D)** Auto- and cross-correlations (1 ms bin size) of three opto-identified Barr^{CRH} neurons with their average spike waveforms showing isolation and a degree of cross-correlation at short latency.

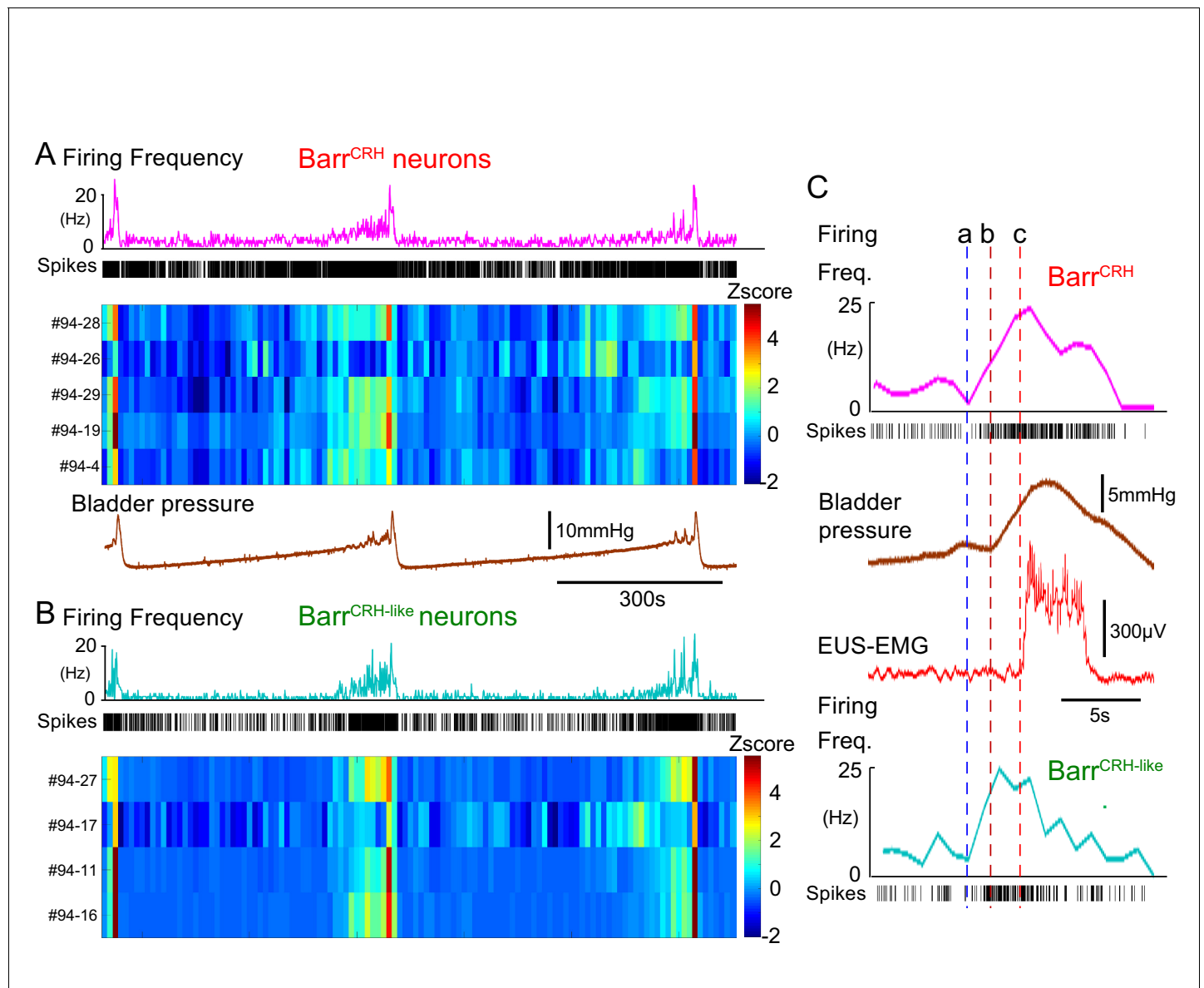


Figure 9. Barr^{CRH} neuronal firing anticipates bladder pressure during the micturition cycle. (A) Barr^{CRH} neurons showed a bursting pattern of discharge that aligned with bladder pressure. The z-scored responses of all Barr^{CRH} neurons in this recording can be seen to have a similar pattern of activity (single representative firing rate plot shown above). (B) Within the same recording (and from adjacent probe sites) a further group of neurons was noted ($n = 4$) to exhibit a similar pattern of bursting discharge synchronized to the voiding cycle. These neurons were termed Barr^{CRH-like}. Auto and cross-correlations of the Barr^{CRH-like} and Barr^{CRH} neurons (see **Figure 9—figure supplement 1**) showed them to have similar properties and evidence of a degree of short latency correlation to other Barr^{CRH-like} neurons and also Barr^{CRH} neurons. (C) The increase in firing activity (a) of both Barr^{CRH-like} and Barr^{CRH} neurons (same experiment), preceded and anticipated the change in bladder pressure (b) and occurred before the onset of voiding marked by the sudden increase in EUS-EMG (c).

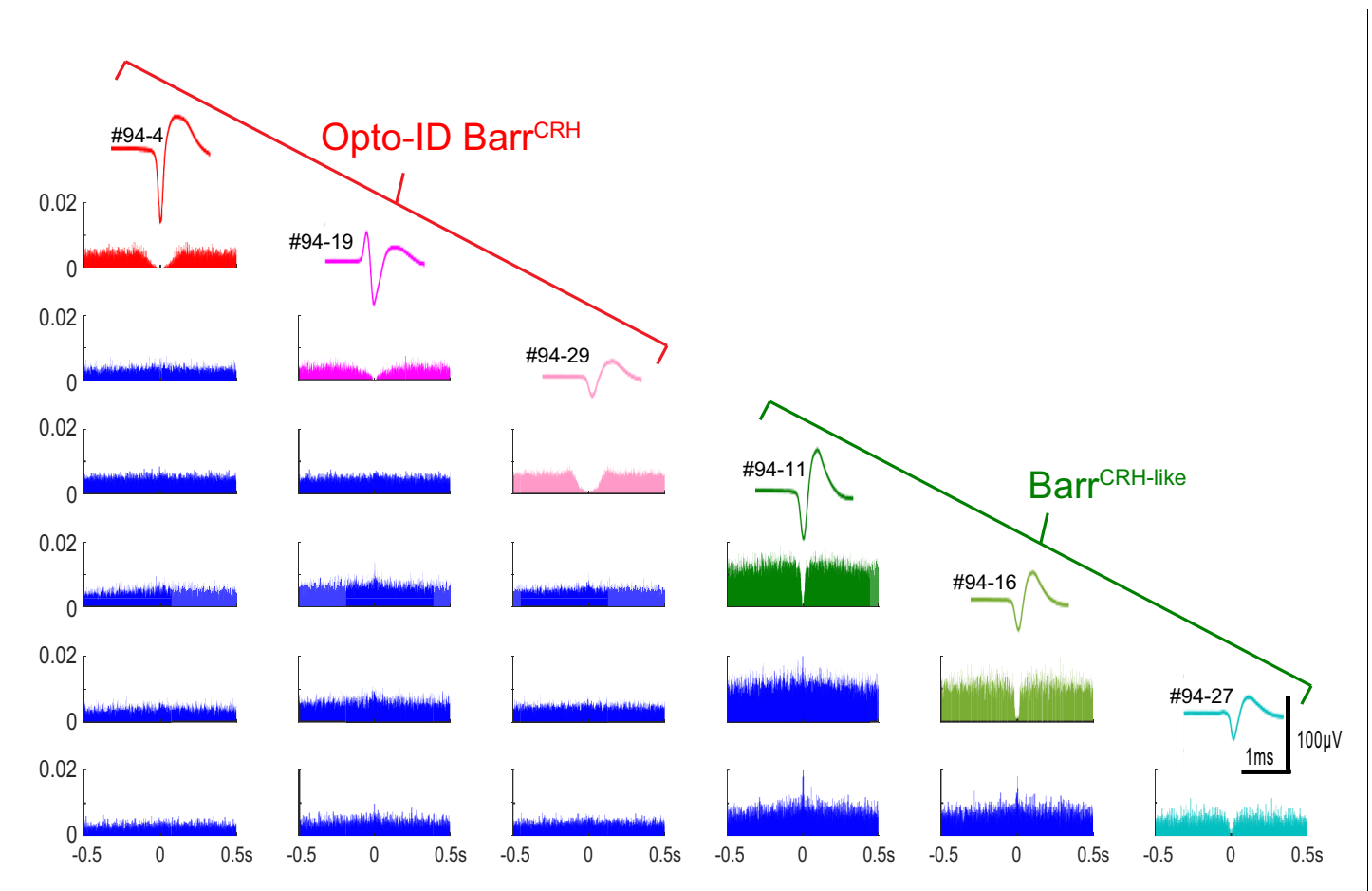


Figure 9—figure supplement 1. Auto- and cross-correlations of $Barr^{CRH}$ and $Barr^{CRH-like}$ neurons. $Barr^{CRH}$ and $Barr^{CRH-like}$ neurons ($n = 3$ per group) recorded in the same mouse showing their distinct spike waveforms and autocorrelations with a marked central valley feature indicating that they each represent a discriminated unit. The cross-correlations show that several of the units have a short latency cross-correlation indicating that they tended to fire together in synchrony and such cross-correlations were noted both within and between the $Barr^{CRH}$ and $Barr^{CRH-like}$ neuronal groups.

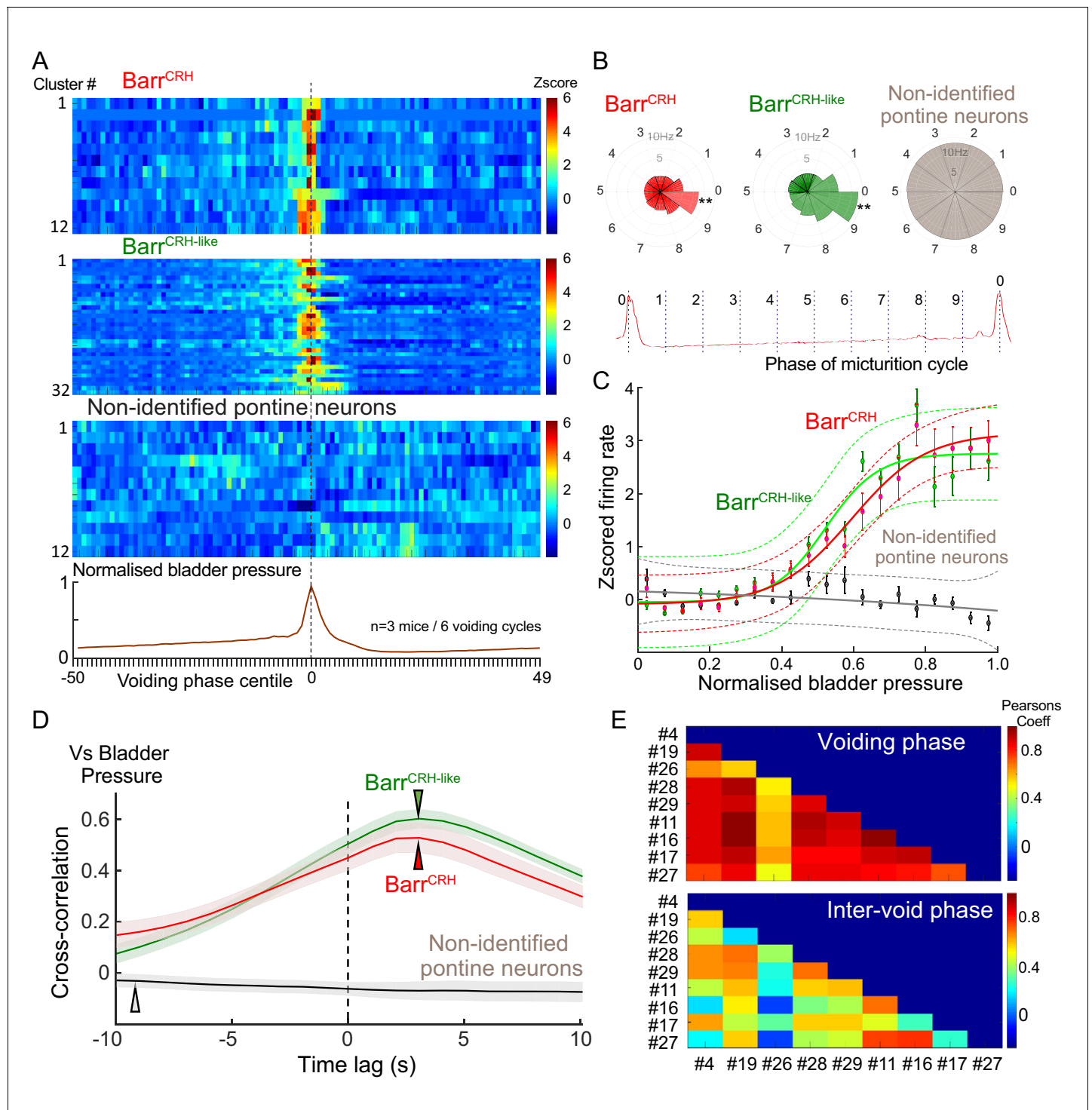


Figure 10. Population dynamics of Barr^{CRH} and Barr^{CRH-like} neurons. (A) Firing rate heat maps from probe recordings across mice ($n = 3$) with opto-identified Barr^{CRH} neurons ($n = 12$, (respectively 8, 3 and 1 in each mouse)) and Barr^{CRH-like} neurons ($n = 32$, (respectively 9, 19 and 4 in each mouse)) showed very similar patterns of firing in relation to the voiding cycle (shown below normalized for pressure and time across six cycles). (B) Rose plots of firing activity against phase of micturition cycle showing that both Barr^{CRH} and Barr^{CRH-like} neurons increase their firing in the phase decile leading up to the void unlike the unidentified neurons (**- $P < 0.01$, one-way ANOVA followed by Tukey-Kramer test). (C) Plotting the relationship between firing rate and normalized bladder pressure showed a graded sigmoid relationship with increased firing rate corresponding to higher bladder pressures. No such relationship was seen for the other neurons in the dorsal pons (dotted lines mark 95% CI of curves, bars SEM of firing rate) (D) The cross correlation between Barr^{CRH} (and Barr^{CRH-like}) neurons and bladder pressure was strongest at a lag of 3 s indicating that the bladder pressure follows the change in

Figure 10 continued on next page

Figure 10 continued

neuronal firing (shaded area marks SEM of mean cross correlation) (E) Colour plots of the Pearson's cross-correlation coefficient between pairs of the population of Barr^{CRH} and Barr^{CRH-like} neurons is consistently strongest in the voiding phase.

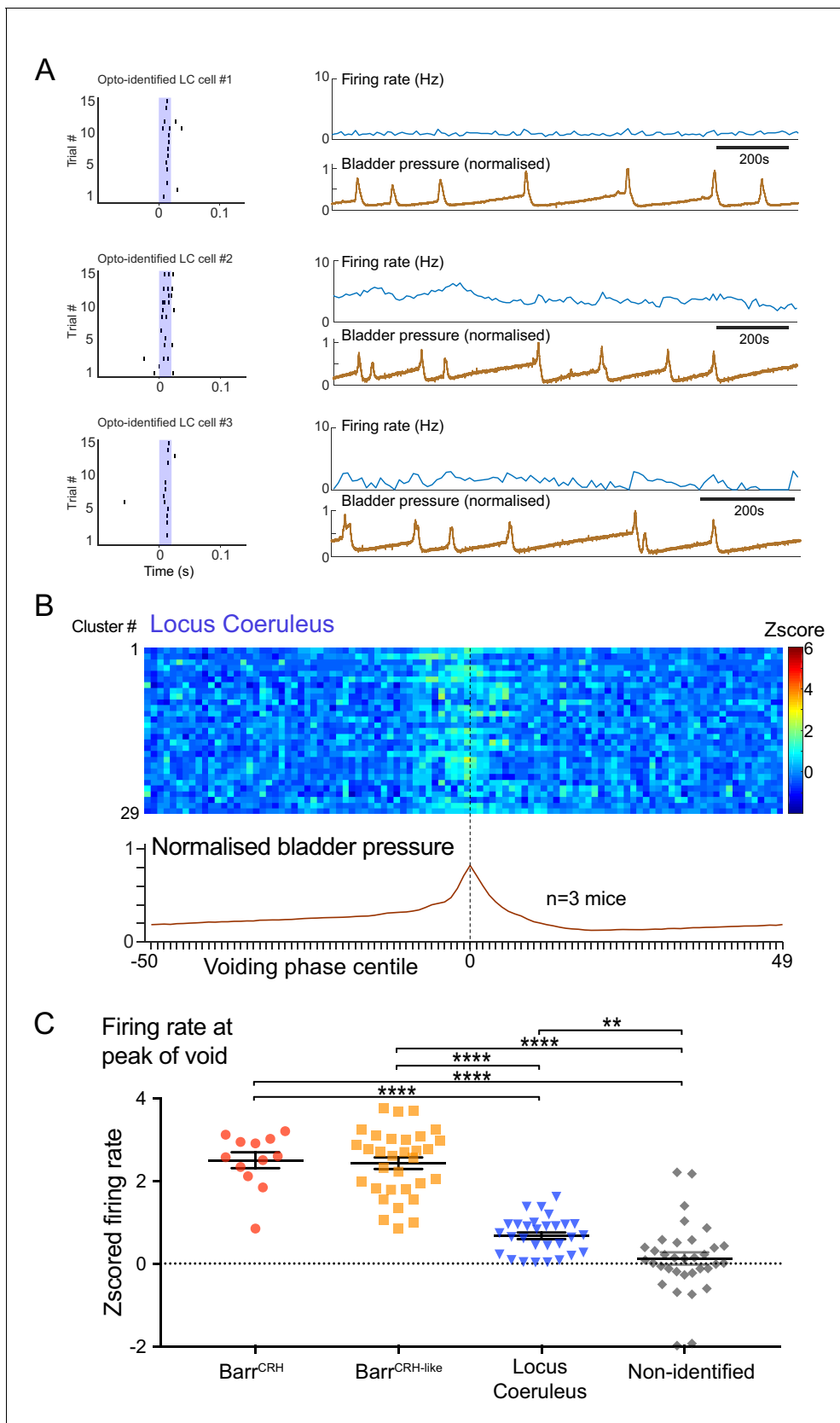


Figure 10—figure supplement 1. Dynamics of Locus coeruleus neurons with respect to the micturition cycle. (A) Recordings of opto-identified LC neurons showing entrained firing responses to blue light illumination (20 ms) and firing rate increases during the voiding contractions. (B) Firing rate Figure 10—figure supplement 1 continued on next page

Figure 10—figure supplement 1 continued

heat maps (zscored) from recordings across mice ($n = 3$) with opto-identified LC neurons ($n = 29$) showed an increase in firing during the voiding phase (normalized bladder pressure across 3–6 voiding cycles). (C) Comparison of the increase in firing (zscored and averaged across five central centile bins centred on bladder pressure peak) showing that the Barr^{CRH} and Barr^{CRH-like} neurons have a greater increase in firing than LC neurons which in turn show a greater increase than the non-identified group (ANOVA with Holm-Sidak's post hoc test, **** $p < 0.0001$, ** $p < 0.01$). Source data in **Figure 10—figure supplement 1—source data 1**.

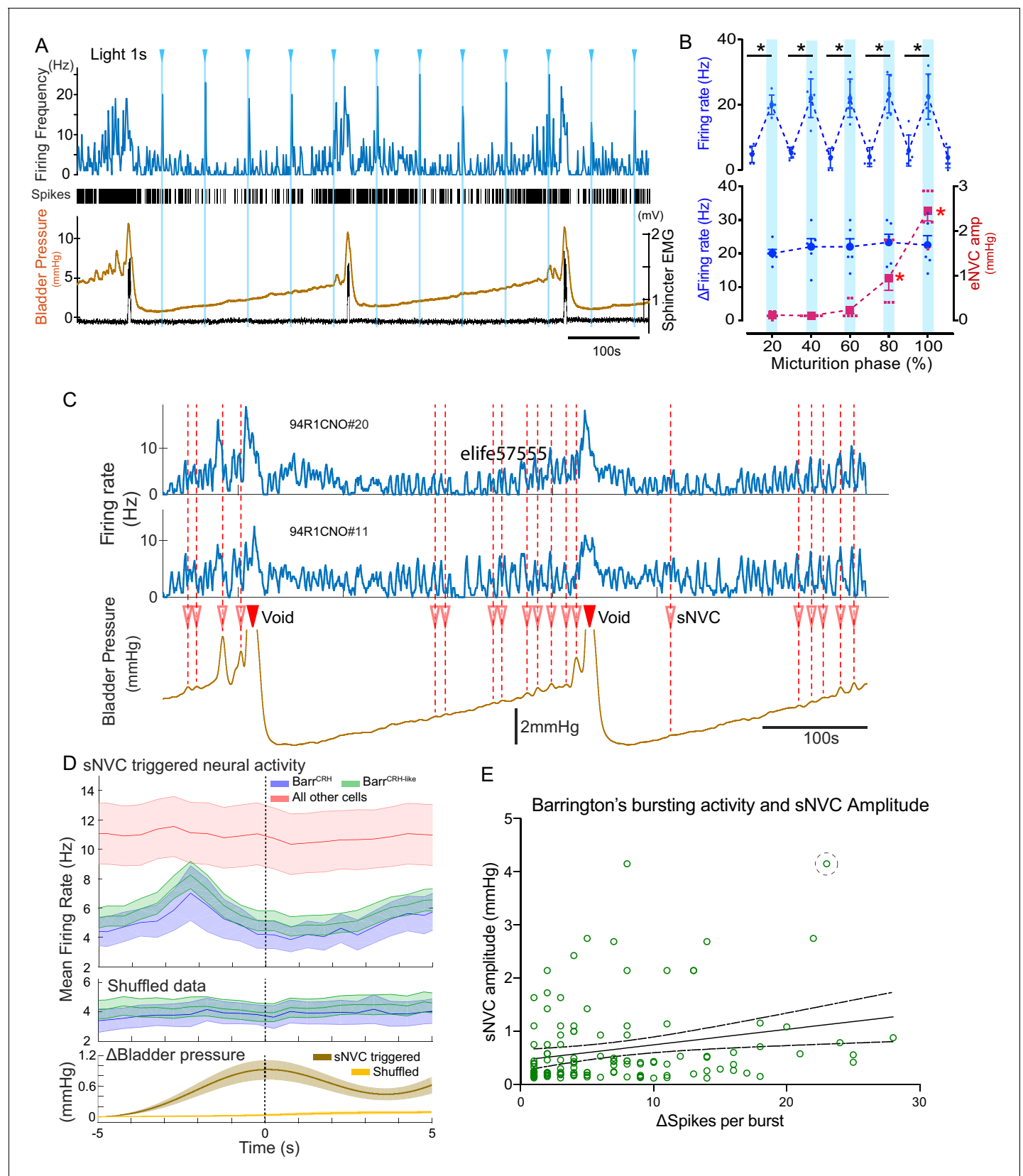


Figure 11. Barr^{CRH} neuronal activity conditionally drives bladder pressure. (A) Optogenetic stimulation of Barr^{CRH} neuron showing the transient increases in firing evoked by light pulses (1s × 465nm, pale blue lines) applied at different points of the micturition cycle. (B) Pooled data from Barr^{CRH} Figure 11 continued on next page

Figure 11 continued

neurons ($n = 6$ across three mice) showing that there was no difference in firing (either the peak firing rate (upper) or the change in firing (lower, blue circles)) evoked by light across the phases of the micturition cycle. In contrast the amplitude of the eNVC (see **Figure 3**) increases markedly across the micturition cycle. (red squares) (C) Spontaneous NVCs were identified using a peak finding algorithm (amplitude 0.1–4 mmHg, green dotted circles) and were noted to be preceded by a burst of Barr^{CRH} activity. (D) Averaged firing rate plots of Barr^{CRH} and Barr^{CRH-like} neurons triggered off sNVCs (averaged bladder pressure trace at the bottom) showed a consistent burst of firing between 1.5–3 s before the onset of sNVCs (unlike the unidentified population). Note this relationship was not seen in the shuffled data. (Mean firing rates \pm S.D, 0.5 s bins). (E) Linear regression showed the number of spikes in each Barr^{CRH} burst only showed a weak correlation (slope 0.03 mmHg/spike) with the amplitude of the following sNVC. This weak relationship was lost if a single outlier point was excluded (ringed). Source data in **Figure 11—source data 1**.

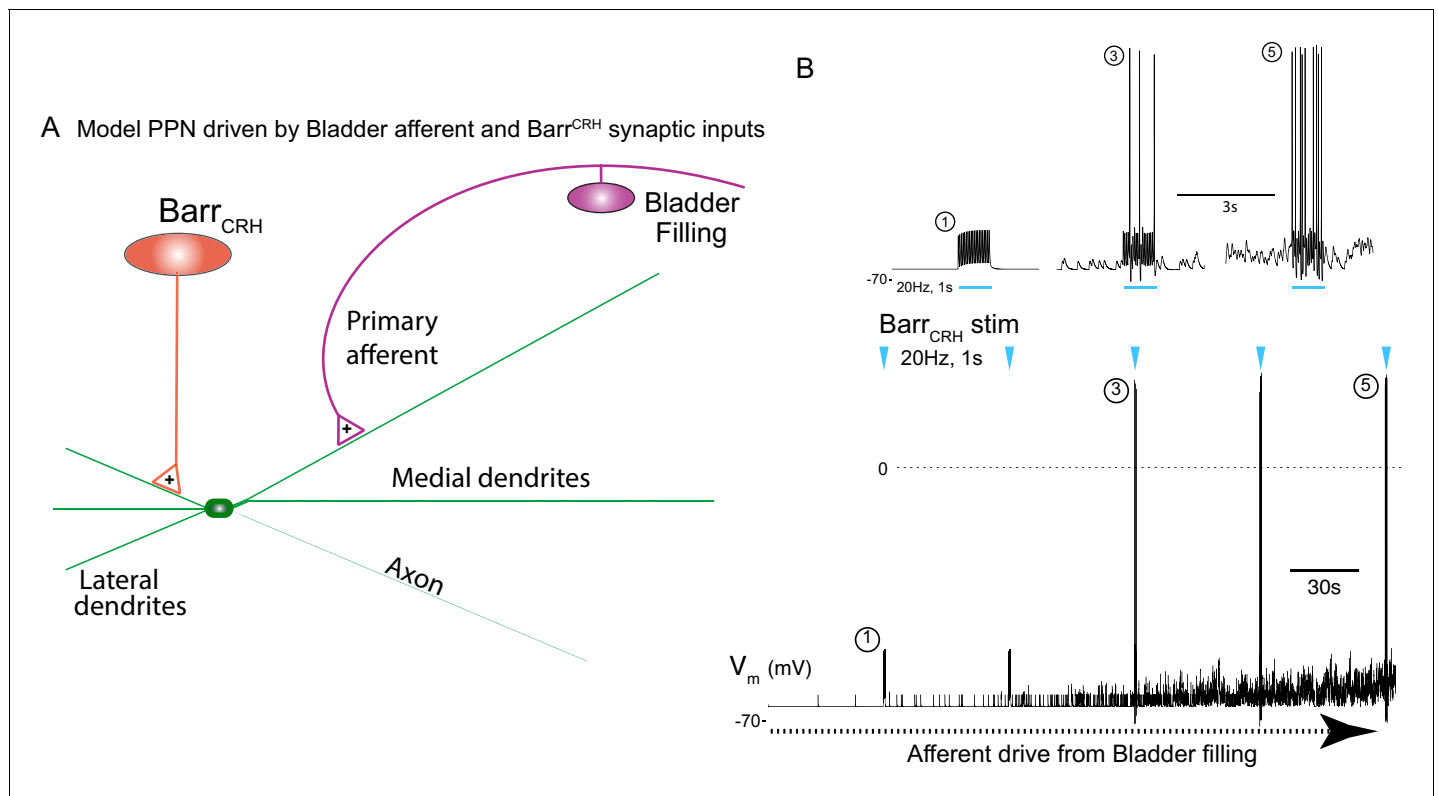


Figure 12. Integrative model of Barr^{CRH} drive to bladder parasympathetic neurons in micturition cycle. (A) Model of a parasympathetic preganglionic neuron (implemented in NEURON) with a synaptic drive from Barrington's nucleus and a second synaptic input from a bladder afferent neuron. (B) The model PPN is depolarised as the firing of the afferent neuron increases with bladder distension (afferent input from recordings *Ito et al., 2019*) producing an augmenting synaptic excitation (subthreshold for spike firing). Coincident 20 Hz stimulation of the Barr^{CRH} neuron (blue arrow heads, mimicking opto-activation) evokes no parasympathetic spike output at the start of the cycle but this increases to 8–10 Hz by the end of the cycle (traces shown on expanded timebase above).

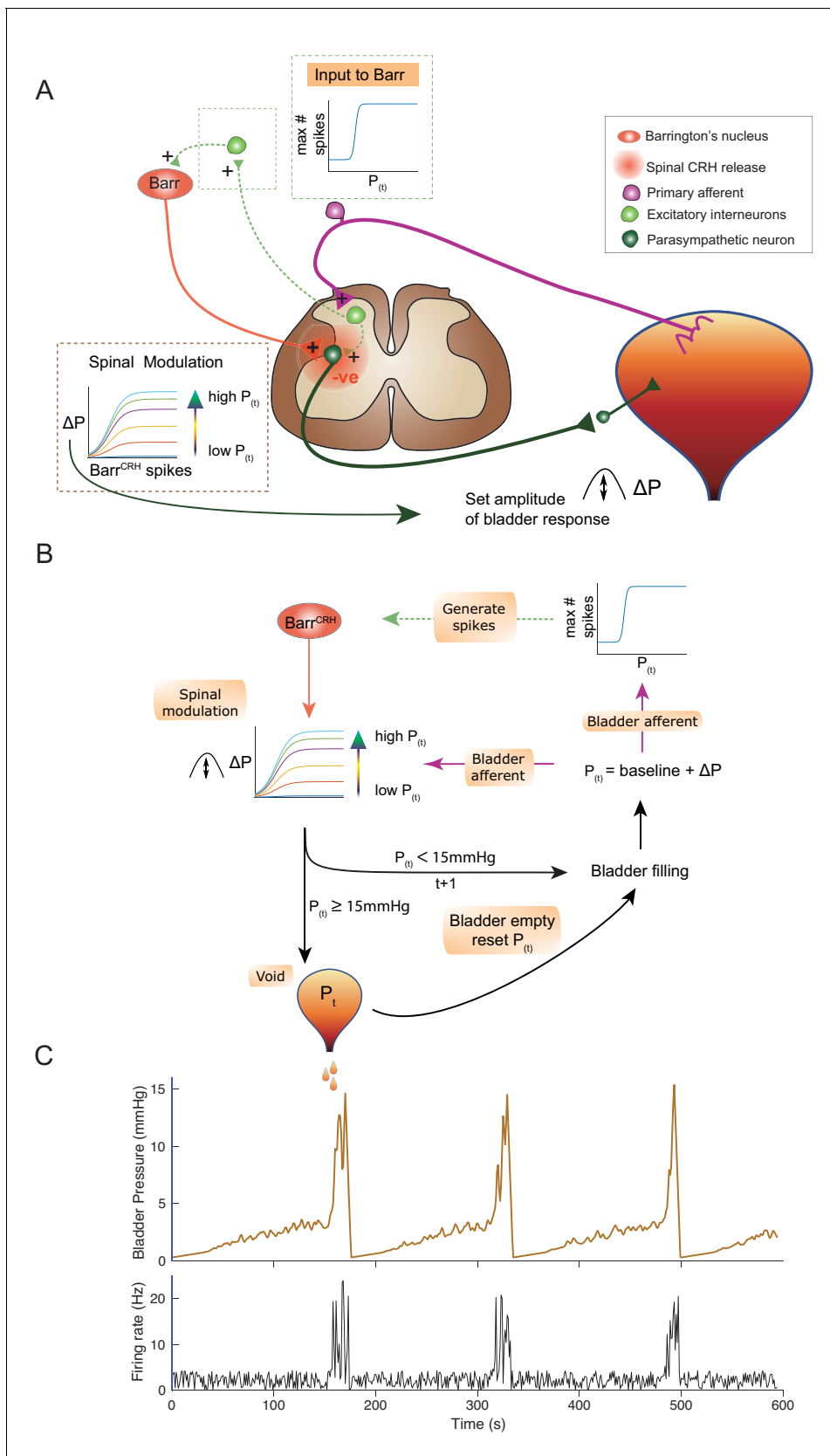


Figure 13. An inferential model of autonomous micturition. (A) Schematic of the descending input from Barrington's nucleus to the bladder parasympathetic neurons. The parasympathetic neurons receive excitatory input from bladder afferents – shown as being relayed via a segmental Figure 13 continued on next page

Figure 13 continued

excitatory interneuron. Note that the Barr^{CRH} neuron has both a fast, excitatory transmitter (presumed glutamate) as well as an inhibitory action mediated by spinally released CRH – possibly acting via local inhibitory interneurons (not shown). The inset boxes show the logistic relationships linking activity of Barr^{CRH} neurons and spinal excitability to the current bladder pressure (from model in B). (B) Flow chart showing processing steps in inference model of micturition. (C) Output from the model showing incrementing bladder pressure with NVCs over three micturition cycles with the associated Barr^{CRH} firing that generates the NVCs and the voids.

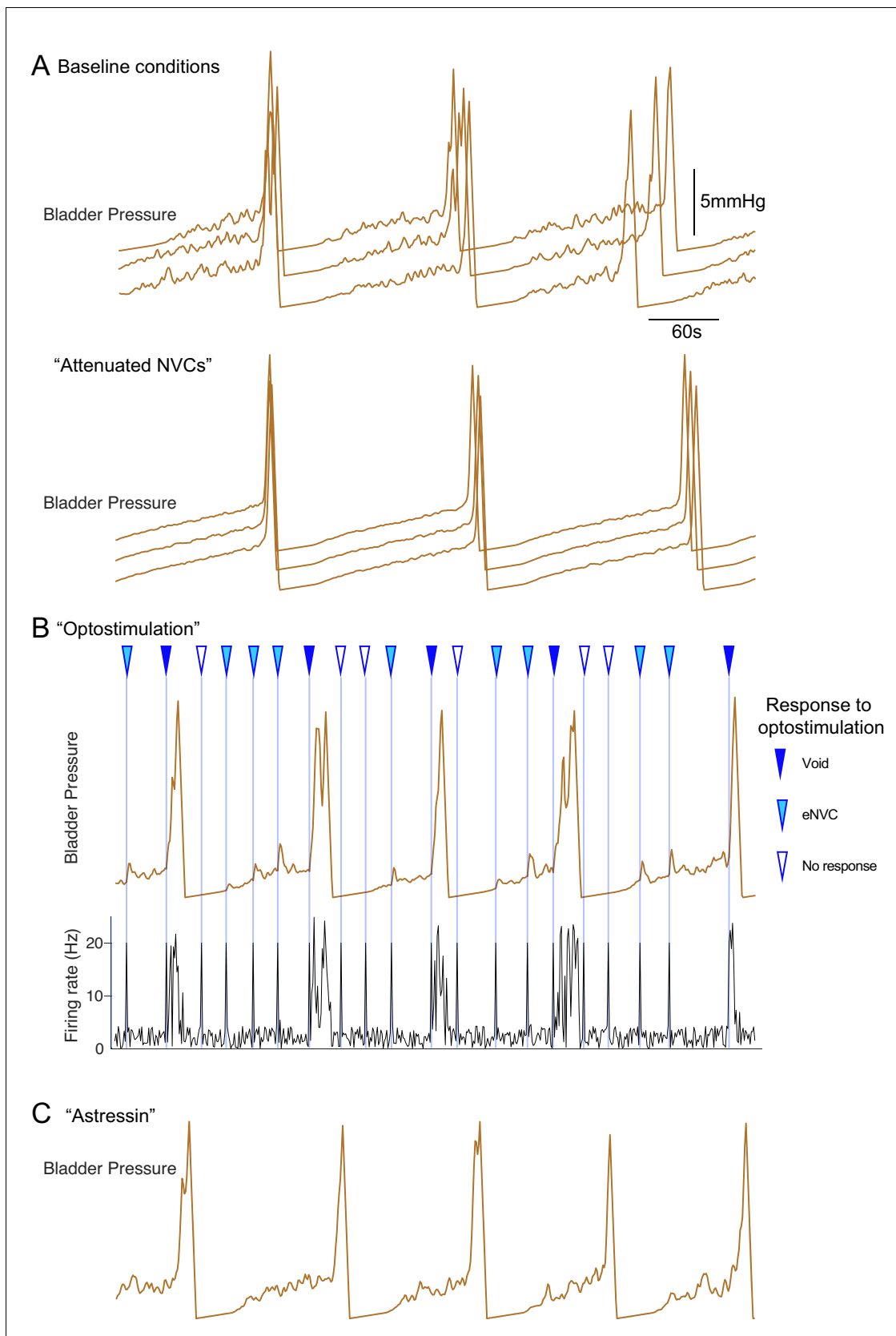


Figure 13—figure supplement 1. Inferential micturition model recapitulates observed behaviour. (A) Comparison of model outputs under basal conditions (upper panel, three consecutive runs) with a reduction in the variability in the Barr^{CRH} firing (mean rates unchanged, lower panel). This Figure 13—figure supplement 1 continued on next page

Figure 13—figure supplement 1 continued

attenuates the amplitude of the NVCs and delays the time to void indicating the importance of the NVCs in the micturition cycle. **(B)** Simulation of optogenetic activation of Barr^{CRH} neurons (20 Hz x 1 s) at different points in the micturition cycle (all other model parameters as the basal condition in A). This external drive increased micturition frequency by triggering voids (when stimuli fell later in the filling cycle). Note that opto-activation earlier in the filling cycle generated NVCs of varying amplitude and also could lead to 'failures' with no bladder contraction. **(C)** A leftward shift in the mid-point (by 1 Hz) of the spinal modulation sigmoid mimicked the effect of CRH antagonist astressin by increasing the excitability of the spinal circuit. This increased the amplitude of NVCs and increased micturition frequency (as compared to the basal condition shown in A).